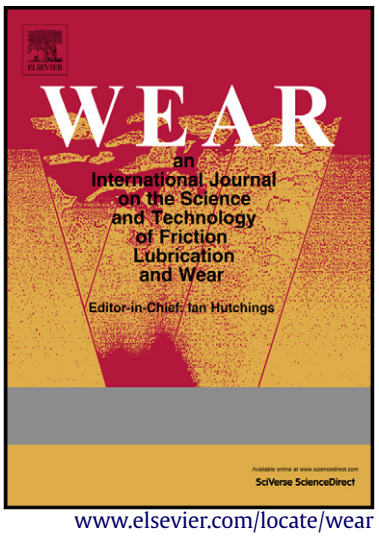

www.elsevier.com/locate/wear

Effect of impact Angle on the slurry erosion-corrosion of Stellite 6 and SS316

N. Andrews, L. Giourntas, A.M Galloway, A. Pearson

PII: S0043-1648(14)00264-6
DOI: http://dx.doi.org/10.1016/j.wear.2014.08.006
Reference: WEA101088

To appear in: *Wear*

Received date: 7 April 2014
Revised date: 1 August 2014
Accepted date: 9 August 2014

Cite this article as: N. Andrews, L. Giourntas, A.M Galloway, A. Pearson, Effect of impact Angle on the slurry erosion-corrosion of Stellite 6 and SS316, *Wear,* http://dx.doi.org/10.1016/j.wear.2014.08.006

Effect of impact angle on the slurry erosion-corrosion of Stellite 6 and SS316

N. Andrews[a] *, L. Giourntas[a] , A. M Galloway[a], A. Pearson[b]

[a] Department of Mechanical & Aerospace Engineering, University of Strathclyde, Glasgow, Scotland

[b] Weir Engineering Services, Oil & Gas Division, East Kilbride, Glasgow, Scotland

*Corresponding Author:
Nicola Andrews
M19A, James Weir Building
Department of Mechanical and Aerospace Engineering
75 Montrose Street,
Glasgow
G1 1XJ
n.andrews0401@gmail.com
Contact Number: +44749552599

Additional Authors:
Lampros Giourntas: lampros.giourntas@strath.ac.uk
Dr Alexander Galloway: alex.galloway@strath.ac.uk
Alastair Pearson: a.pearson@weirservices.co.uk

Effect of impact angle on the slurry erosion-corrosion of Stellite 6 and SS316

N. Andrews[a], L. Giourntas[a], A. M Galloway[a], A. Pearson[b]

[a] Department of Mechanical & Aerospace Engineering, University of Strathclyde, Glasgow, Scotland

[b] Weir Engineering Services, Oil & Gas Division, East Kilbride, Glasgow, Scotland

Abstract

This study is an investigation of the effect of impingement angle on slurry erosion-corrosion of Stellite 6 manufactured by sand casting, lost wax casting and SS316. The tests were performed using an impingement rig in which a slurry with 3.5% NaCl and 1.177g/l suspended angular sand particles at 19m/s were recirculated for one hour. The results were obtained for angles of 20°, 45°, 60° and 90° to the exposed surface. Post experimental analysis using light microscopy, surface profiling and SEM assisted with clarification of the wear mechanisms and assessment of the severity of surface damage. Stellite 6 consistently exhibited superior wear resistance compared with SS316. The most severe regime for SS316 was experienced at low angle of impingement, 45°, due to its ductility. Alternatively, the brittle network of chromium carbides showed significant impact on the behaviour of cast Stellite 6 under solid-liquid impingement with the most critical erosion-corrosion damage occurring at 60°.

Keywords: slurry erosion, erosion testing, steel, non-ferrous metals, surface analysis

1. Introduction

Erosion-corrosion is a form of material degradation involving mechanical wear coupled with electrochemical corrosion processes. This phenomenon generally occurs in components that transport corrosive slurries, such as pipe work, pump casings, impellers, valves etc. The erosion-corrosion occurrence can be very destructive on equipment and components that come into contact with corrosive slurries and may contribute significantly to problems such

as loss of efficiency, increased maintenance costs and possible catastrophic failure leading to total breakdown.

Stellite 6, a cobalt based Corrosion Resistant Alloy (CRA) alloy with a hard chromium carbide phase, is used extensively for industrial applications where the components are exposed to highly erosive and corrosive conditions. CRA's are a group of materials that form a passive oxide film providing protection to the metals against corrosion and include other commonly used materials such as SS316.

The interaction of erosion and corrosion has been studied as the combined mass loss of pure erosion (E) and pure corrosion (C) which does not equate the total mass loss (T) when a material is exposed to both simultaneously [1]. The mass loss attributed to the interaction of the electrochemical and mechanical processes is named the 'synergistic' effect (S). The equation for this erosion-corrosion phenomenon is deduced in Equation 1.

$$T = E + C + S \qquad \text{Equation 1}$$

The total mass loss was recorded in this study but the effect of corrosion and synergy were not individually investigated.

Neville and Hodgkiess [2] have studied the performance of Stellite 6 in perpendicular angle of attack under solid-liquid impingement compared with Superduplex and Inconel 625. In their work, Stellite 6 showed similar erosion-corrosion resistance in solid-liquid impingement with Inconel 625 and slightly better than Superduplex. Neville et al [3] also reported good erosion-corrosion behaviour of Stellite X40 in saline solutions when the solid loading of the liquid impingement jet is low or negligible. Stellite X40, as a part of the Stellite family, gives an indication of the erosion-corrosion performance of Stellite 6 under solid-liquid impingement and renders this significant for the present study.

Yu et al. [4] have evaluated the abrasive wear resistance of sand cast and hot isostatically pressed (HIPed) Stellite 6 in a dry sand rubber wheel abrasion test rig. The results showed that both cast and HIPed Stellite 6 had no significant difference in their wear resistance. Malayogu and Neville [5] reported on similar work on sand cast and HIPed Stellite 6 by comparing their erosion-corrosion performance with two stainless steels in perpendicular angle of impingement. The results proved that Stellite 6 generally possesses better erosion-

corrosion performance, especially HIPed Stellite 6, which showed superior erosion-corrosion performance compared to all comparative materials.

The angle of impingement aspect of this current work refers to the angle between the eroded surface and the particles impacting on that surface which has previously been reported by Stachowiak et al [6]. Angle of impingement is an important industrial consideration as slurry erosion handling components such as piping systems, valves and impellers experience impacting erosive particles in a full spectrum of angles. The severity of the erosion performance of the material is highly dependent on its ductility. Stellite 6 is a predominantly ductile material but the cast structure is composed of a network of brittle chromium carbides, thus the wear mechanism at varying angles of impingement is unknown. Ninham [7] investigated the response of numerous metals including Stellite 6 using silicon carbide particles as the erodent in dry erosion at 30^{o}, 60^{o} and 90^{o}. This research [7] resulted in the maximum erosion rate occurring at 60^{o} impingement but the material was not exposed to a saline solution therefore not considering the effect of erosion-corrosion.

Burstein and Sasaki investigated the erosion-corrosion mechanism at oblique angles between 10^{o} and 90^{o} of 304L Stainless Steel [8] under 0.8 wt% slurry and 0.6 M NaCl aqueous solution. SS304L is a ductile material and it demonstrated [8] a peak mass loss between 40^{o} and 50^{o}. As SS304L and SS316 are both austenitic stainless steels, the results can possibly be used as an indicator to the response of SS316 in the current study. The effect of particle velocity and impact angle on SS304 and the martensitic SS420 has also been documented at 30^{o} and 90^{o} in a slurry composed of 0.5 M H_2SO_4 + 3.5% NaCl and 30 wt% quartz particles at fluid velocity of 4.5 m/s and 8.5 m/s [9]. Interestingly, harder martensitic stainless steel, SS420, presented a significant corrosion influence giving a lower overall erosion-corrosion resistance than SS304. In this testing regime corrosion was a more relevant factor than hardness. This research [9] verifies that the most severe regime for stainless steels, both martensitic and austenitic, is at an acute angle of 30^{o} and high velocity of 8.5m/s.

The present study is highly novel in that the effects of impact angle on two manufacturing routes of Stellite 6 (sand cast and lost wax) and SS316 have not been investigated in

erosion-corrosion conditions. Measured against the reference material, SS316, the key objective of this study was to compare the erosion performance of the two Stellite 6 manufacturing/casting routes under various angles of impingement. Hence, this comparator study reports on the corrosive wear mechanisms of Stellite 6 manufactured by two different casting techniques. The high NaCl content slurry was used to develop the electrochemical processes and the mechanical damage processes were generated by the inclusion of angular sand particles within the slurry. The angles of impingement were 20^{o}, 45^{o}, 60^{o} and 90^{o}.

2. Experimental

The main experimental phase of this study concentrated on the erosion-corrosion phenomena and the materials studied (sand cast Stellite 6, lost wax cast Stellite 6 and SS316) were initially characterised using light microscopy and Scanning Electron Microscopy (SEM) with a 20kV accelerating voltage and secondary electron detector. Hardness testing was conducted on each specimen using a standard Vickers Hardness Testing machine with a 20kg load.

This comparator study focused on two different methods of casting Stellite 6; lost wax casting and sand casting. In both cases, the cast alloy forms a classic dendritic type structure as a result of the typically sluggish solidification process in which the cast alloy exhibits a hypoeutectic microstructure in which the primary Co-rich dendrites are surrounded by Cr-rich M_7C_3 (M=Metal) eutectic carbides in a solid solution cobalt matrix [10]. Evidence of these carbides is clearly shown in Figure 1 from an energy dispersive x-ray analysis in a region of lost wax cast Stellite 6. In terms of bulk chemical analysis, an SEM average analysis over a cross-sectional area encompassing both Cr-rich carbides and the Co matrix provided the chemical composition of both lost wax cast and sand cast Stellite 6 and compared well with the proprietary chemical analysis available in the literature [4, 10]. Lost Wax Cast Stellite 6 is 38%Cr, 54%Co, 6%W, 2%Fe and Sand Cast Stellite 6 is 30%Cr, 61%Co, 6%W, 1.26%Fe, 0.8%Mn, 0.9%Si. The hardness values of Lost Wax Cast and Sand Cast Stellite 6 are $394HV_{(20)}$ and $386HV_{(20)}$ respectively. SS316 had a recorded hardness of $186HV_{(20)}$.

The two Stellite 6 casting methods presented similar microstructures; Figure 1 displays the 2-phase microstructure of lost wax cast Stellite 6. The dark grey areas are Cr-rich carbides and the light grey areas represent the cobalt-rich matrix. A small percentage of carbon is combined with tungsten and it results in tungsten carbides which were confirmed by the SEM spot inspection of the white areas in Figure 1. A spot analysis was also used to determine the composition of the chromium carbide areas and cobalt matrix for each casting technique which is presented in Table 1.

Figure 1: Typical Lost Wax Cast Stellite 6 microstructure (SEM photo)

Table 1: Compositional analysis of Stellite 6

The erosion-corrosion performance of the comparator materials was assessed using a re-circulating impinging jet apparatus which is shown in Figure 2. The nozzle delivered solid-liquid slurry to the specimen surface at velocity of 19m/s. The nozzle diameter was 3.8mm and offset from the specimen by 5mm. The exposed surface of each test specimen to impingement was 25mm^2 and grinded using an incrementally finer grade of silicon carbide paper through 120, 220, 500 and 800grit. Each specimen was weighed before and after the experiment using a mass balance of accuracy 0.1mg. The experiments involved a one hour exposure in which the temperature rose from 10^o to 20^{o}C.

Figure 2: Schematic diagram of the re-circulating apparatus

The specimen holder was altered to attain solid-liquid impingement angles of 20, 45, 60 or 90^o. At each angle, the specimens were exposed to 3.5% NaCl solution with 1.177g/l suspended angular sand. The distribution of sand particle size was measured by using incrementally finer mesh size sieves, the range is shown in Figure 3. The sand concentration in the slurry was regularly checked by filtering, drying and weighing the sand throughout the experiment.

Figure 3: Distribution of particle size of sand used in liquid-solid slurry

A comprehensive post-experimental study of the specimen surfaces was conducted. The impingement area was reviewed using an Olympus ZX51 light microscope and Hitachi S-3700 SEM. This enabled an understanding of micro-structural degradation across the wear scar. A SV-2000 Surface profiler was used to ascertain the depth of the erosion-corrosion wear scar in the impingement area of each specimen. A diamond pin was moved across the

specimen measuring any variance in depth on the surface. The results of this motion are displayed as a 2-Dimensional profile scan.

3. Results

3.1 Liquid-solid experiments with different angles of impingement

The effect of various angles of impingement with each tested material under the liquid-solid slurry is shown numerically in Table 2 and graphically in Figure 4. The mass loss was averaged over four replicates of the same environment to take account of variations within the results.

Table 2: Mass losses of each material as a function of angle of impingement

Figure 4: Average Mass Loss of Stellite 6 and Stainless Steel 316 with varying angle of impingement

According to Figure 4, Co-based alloys demonstrate a superior erosion-corrosion resistance compared to SS316. SS316 also shows the behaviour of ductile materials in experiencing the greatest material loss at relatively shallow angles of impingement. An interesting feature of the mass losses is that, whilst for stainless steel this is maximum at 45^{o} – with a clear decrease between 45^{o} and 60^{o}, the material loss for Stellite is either similar or greater at 60^{o} than at 45^{o}. This feature may be associated with the relatively complex microstructures of Stellite in that cast Stellite 6 has a ductile matrix but an extensive network of brittle chromium carbides, which may be exerting a significant influence on the erosion-corrosion performance.

The Vickers hardness of the test specimens was considered as a factor which would influence the erosion-corrosion performance. The correlation between hardness and erosion-corrosion performance is shown in Figure 5 presenting two noteworthy trends. Firstly, as the hardness of the material increases there is greater erosion-corrosion resistance. The hardness of lost wax and sand cast Stellite 6 is 394$HV_{(20)}$ and 386$HV_{(20)}$, respectively, whilst the SS316 was found to have a hardness of 186$HV_{(20)}$. Secondly, the steepest gradient lines are recorded at 45^{o} and 20^{o} impingement angle indicating that hardness has a greater significance when erosive fluid is grazing over the exposed material surface.

Figure 5: Correlation between Vickers hardness and average mass loss at varying angles of impingement

3.2 Post experimental analysis

3.2.1 Macroscopic/Microscopic Imaging

The exposed surfaces are significantly different between the varying angles of impingement. The perpendicular impingement wear scar for SS316 is shown in Figure 6(a). The wear scar is symmetrical with the most severe degradation of the surface occurring at the central impingement area. As the angle of impact tends to low angle of impingement at 20^{o} the sand particles are abrading over the surface producing an elongated wear scar. The transition from high to low angle of impingement is clearly depicted in the macro images of the wear scars for SS316 in Figure 6.

Figure 6: Macro Image of SS316 wear scar at 90^{o} (a), 60^{o} (b), 45^{o} (c), 20^{o} (d)

Figure 7 illustrates the characterisation of wear scars. Light microscopy was used as a method to understand the extent of degradation of the microstructure at varying areas of the exposed surface.

Figure 7: Characterisation of impingement at 90^{o}

Impingement area A is the section of the surface where the flow of slurry has directly impinged upon the material; the microstructure in this area will suffer the highest degradation. Area B shows directionality in the degradation of the surface due to the turbulence caused by impinging sand particles. Area C presents random directionality of the microstructure which can be attributed to both corrosion and sliding abrasion.

The perpendicular incidence of particles develops craters and pits in the direct impingement area A. The turbulent disruption of fluid flow causing directional destruction of the metal matrix is evident in Figure 8, Area B. Area C, presents random marks across the outer area due to sliding abrasion; although the microstructure remains noticeably intact.

Figure 8: Surface Structure Lost Wax Cast Stellite 6, 90^{o}

The grazing impact at low angle of impingement produces directionality in the degradation of the surface. The hard chromium carbide phase presents higher resistance to wear than the cobalt matrix and thus is distorted but not completely removed during erosion-corrosion testing. Sliding abrasion emerges as the main mechanism for material removal at 20^{o} producing an elongated wear scar. The turbulent region (Area B) and outer region (Area C) suffer a lower degree of degradation compared with 90^{o} impingement potentially due to the sand particles producing a lack of turbulence around the direct impingement area. Figure 9 presents the wear scar across the surface of the lost wax casting, Stellite 6 at 20^{o} angle of impingement.

Figure 9: Surface Structure Lost Wax Cast Stellite 6, 20^{o}

Figure 10 depicts the degradation of the microstructure of SS316 across the wear scar at 45^{o} where the greatest mass loss was recorded.

Figure 10: Surface Structure SS316, 45^{o}

3.2.2 Surface Topography

Surface profiling is a useful tool to determine the maximum wear depth and distribution of mass loss across the exposed surface. The maximum wear depth for each respective material at each impact angle was determined using 4 scan replications and the greatest depth recorded. There is a direct correlation between greatest wear scar depth and maximum mass loss as expected. The surface profile for the most severe regime of SS316 (45^{o}) and Sand Cast, Stellite 6 (60^{o}) are depicted in Figure 11 and 12.

Numerically the maximum cross-section profile wear depth for Stainless Steel 316 is Y = 194.36µm and for Stellite 6 is Y = 104.78µm.

Figure 11: 2D surface profile scan of SS316 at 45^{o}

Figure 12: 2D surface profile scan of Sand Cast Stellite 6 at 60^{o}

Elongation of the wear scar shown in the macroscopic images can be numerically analysed using surface profiling scans. The scar dimensions of each material are shown in Table 3.

Table 3: 2D surface profile scan dimensions

The trend between depth of the wear scar and average mass loss at each particular angle of impingement with SS316 is presented in Figure 13.

Figure 13: Correlation of the wear scar depths with the average mass losses of the SS316 at various angles of impingement

Figure 13 highlights the correlation between increasing wear scar depth with increasing mass loss which is upheld for 45°, 60° and 90° to the exposed surface of SS316. The wear scar length should also be considered as it plays a significant role in the analysis. For example, at the shallow angle of 20° SS316 presents low wear scar depth but the impingement length clarifies the reason why SS316 has the second highest mass loss at this angle. A similar correlation is presented with sand cast Stellite 6 at various angles of impingement, shown in Figure 14.

Figure 14: Correlation of the wear scar depths with the average mass losses of the sand casted Stellite 6 at various angles of impingement

The elongated wear scar length at 20° angle of impingement was also recorded with Stellite 6 but the depth is significantly less than SS316. This can be attributed to the increased hardness of Stellite 6 over SS316 providing greater resistance to the sliding abrasion of sand particles. As previously mentioned the ductility of the material has a noteworthy role in a material's response to varying angles of impingement. Stellite 6 exhibits greater erosion-corrosion resistance at both low and high angle of impingement confirming that it can neither be considered an ideally ductile or brittle material. On the other hand, SS316 seems to have a typical ductile response as it tends to have higher mass losses in mainly low angles of impingement [11].

4. Discussion

A number of important aspects relating to Stellite 6 and SS316 under various angles of impingement have been investigated during this study. The metallurgical analysis of the lost wax and sand cast specimens confirmed structural consistency between the two casting processes. Negligible variation was shown between the grain structure of the sand cast and lost wax cast specimens in terms of average grain size and morphology. Also, no difference

could be substantiated between the average mass loss for sand cast and lost wax cast Stellite 6 in each environment.

During the experiment the sand particles are continuously re-circulating and bombarding the specimen surface consequently reducing in angularity. The angular shape of the sand rounds within the one hour test. For this sand shape transformation, it is believed that the erosion rate will be at maximum at the start of the test. Similar events would happen within components that handle erosive-corrosive slurries since the most severe conditions will occur when, for example, a pump is starting and thus the relatively short one hour testing period simulates this effect within the limitations of the rig. A quantity of angular sand was analysed using light microscopy before and after the experiment to quantify how the one hour testing time changes the angularity of the sand. The rounding effect is shown in Figure 15 (a) and (b).

Figure 15 (a) and (b): Reduction in Angularity of Sand Particles during one hour experimental testing

Solid particulates within the slurry significantly increase the mass loss as it is likely to be pure erosion which is the dominant mode of material loss, although not experimentally verified. Stellite 6 showed superior erosion-corrosion resistance compared to SS316 at all angles. At 45^{o} the average mass loss of SS316 is three times higher than the average mass loss of Stellite 6. This can be accounted for by the hardness of Stellite 6 being significantly higher than SS316. The range of hardness variation between Stellite 6 and SS316 had a greater impact on mass loss at grazing impact (20^{o} and 45^{o}) compared with direct impingement (60^{o} and 90^{o}). The impact momentum of angular sand particles is also absorbed due to the toughness of the specimens avoiding brittle fracture at the surface.

The maximum mass loss of typical ductile materials has been documented to increase by a factor of three between perpendicular impact and the most severe regime [7]. This was the result of the current study for SS316 between 45^{o} and 90^{o} presenting an ideal ductile response. Lost wax cast and sand cast Stellite 6 present the maximum mass loss ratio between 90^{o} and their most severe angle of 60^{o} as 2.22 and 2.23 respectively. These experimental results indicate that Stellite 6 can neither be considered an ideally ductile or brittle material.

From the above results, it is clear that erosion-corrosion follows the angular relationships that are associated with pure erosion. Ninham [7] who studied Stellite 6 under dry erosion conditions documented the most severe angle of impingement as 60° which remained true under this current erosion-corrosion study. This outcome indicates that the corrosion component (corrosion and synergy) does not influence the material's behaviour when the angle of impingement is altered.

The post-experimental analysis details the response of the microstructure at varying angles of impingement. The cobalt matrix of Stellite 6 is more susceptible to degradation than the chromium carbide phase hence the reason at 20° angle of impingement a number of chromium carbides remain non-eroded, see Figure 9. At 90° and 60° angles of impingement the main method of material loss was through craters and pitting on the surface but at low angle of impingement (45° and 20°) sliding abrasion causes mechanical wear. The difference in wear mechanism with varying angles of impingement was less obvious with SS316. The outer area surrounding the impingement zone showed pitting and directionality with the flow of particulates but in the central region for all angles the matrix was severely distorted.

Surface profiling indicated that the greatest mass loss and deepest wear scar are interrelated as would be expected. The depth of the wear scar alongside the length of the impingement area provided an indication of the significance of the impingement area with regard to mass loss.

5. Conclusions

From this comparator study, in liquid-solid impingement, the following conclusions can be made.

- Lost Wax Cast and Sand Cast Stellite 6 had similar microstructures and they possessed similar erosion-corrosion resistance. As a result, sand casting can be replaced by Lost Wax casting which provides an improved surface finish product with reduced financial implications.
- The erosion-corrosion results of SS316 and Stellite 6 correspond with the erosion model where the brittle materials are severely damaged mostly in perpendicular

attack and ductile materials suffers mainly in shallow angles (e.g. 20^{o}). Thus, the presence of the corrosion component (i.e. corrosion and synergy) did not alter the trend of erosion damage when the angle of attack is varied.

- SS316 exhibited a ductile response to altering angle of impingement. The greatest mass loss and most severe surface degradation occurred at 45^{o}.
- The cast network of brittle chromium carbides has a significant impact on the response of Stellite 6 to angle of impingement. The greatest mass loss occurred at 60^{o} impingement concluding that Stellite 6 can neither be considered an ideally brittle or ductile material but presented a greater brittle response under this experimental testing.
- Both cast microstructures of Stellite 6 exhibited significant variation in degradation between perpendicular impingement and grazing incidence. The impacting sand particles form pits and craters on the surface at 90^{o} whereas at 20^{o} sliding abrasion appears to contribute to the majority of surface degradation. Under sliding abrasion preferential material removal occurs at the Co-rich matrix.
- Surface profiling indicates that the impingement area is as significant to the mass loss as it is to the maximum depth.

Acknowledgements

The authors would like to acknowledge Weir Engineering Services, Oil and Gas Division, East Kilbride for the financial support provided.

References

1. **X. Hu, A. Neville.** *An examination of the electrochemical characteristics of two stainless steels (UNS S32654 and UNS S31603) under liquid-solid impingement,* Wear, Vol. 256, Issue 5, 2004, p. 537-544.
2. **A. Neville, T. Hodgkiess**. *Characterisation of high-grade alloy behaviour in severe erosion-corrosion conditions,* Wear, Vol. 233-235, 1999, p. 596-607
3. **A. Neville, M. Reyes, T. Hodgkiess, A. Gledhill**. *Mechanisms of wear on a Co-base alloy in liquid-solid slurries*, Wear, Vol. 238, Issue 2, 2000, p.138-150
4. **H. Yu, R. Ahmed, H. de Villiers Love lock, S. Davies**. *Influence of Manufacturing Process and Alloying Element Content on the Tribomechanical Properties of Cobalt-Based Alloys,* Journal of Tribology, Vol. 131. Issue 1,2009, p**.** 011601-1- 011601-12

5. **U. Malayoglu, A. Neville**. *Comparing the performance of HIPed and Cast Stellite 6 alloy in liquid-solid slurries*, Wear, Vol. 255, Issue 1-6, 2003, p.181-194
6. **S.W. Stachowiak, A. W. Batchelor**. *Engineering Tribology, Second Edition,* Abrasive, Erosive and Cavitation Wear, 2001, p. 509-524
7. **A. Ninham**. *The effect of mechanical properties on erosion.* Wear, Vol. 121, Issue 3, 1988, p. 307-324
8. **G. T. Burstein, K. Sasaki**. *Effect of impact angle on the slurry erosion-corrosion of 304L stainless steel.* Wear, Vol. 240, 2000, Issue 1-2, p. 80-94
9. **D. Lopez, J. P. Congote, J. R. Cano, A. Toro, A. P. Tschiptschin**. *Effect of particle velocity and impact angle on the corrosion-erosion of AISI 304 and AISI 420 stainless steel,* Wear, Vol. 259, Issue 1-6, 2005, p. 118-124.
10. **H. Berns, F. Wendl**. *Microstructure and Properties of CoCr29W (Stellite 6) in the As Cast, Forged and Powder Metallurgy Condition,* Cobalt metallurgy and Uses: 2nd Congress, 1985, p.292-305
11. **I. Finnie.** *Some observations on the erosion of ductile metals,* Wear, Vol. 19, Issue 1, 1972, p. 81-90

Material	Cr-rich carbide /wt %			Co-rich Matrix /wt%		
	Cr	Co	W	Cr	Co	W
Lost Wax Cast Stellite 6	73.8	20.7	4.5	27.3	64.8	5.2
Sand Cast Stellite 6	77.3	17.1	5.2	24.8	67.7	4.5

Table 1: Compositional analysis of Stellite 6

Angle of Impingement	Mass Loss/ mg					
	Lost Wax Casting, Stellite 6		Sand Cast, Stellite 6		Stainless Steel 316	
	Test replicates (mg)	Avg (mg)	Test replicates (mg)	Avg (mg)	Test replicates (mg)	Avg (mg)
20	2.8, 2.8, 1.9, 3.0	2.6	2.1, 2.3, 2.4, 3.8	2.3	11.1, 11.3, 11.9, 12.0	11.6
45	3.8, 4.2, 5.4, 5.3	4.7	3.9, 4.0, 4.7, 4.9	4.4	10.1, 12.2, 13.0, 15.0	12.6
60	3.9, 4.3, 5.3, 5.8	4.8	4.6, 5.6, 5.8, 5.9	5.5	8.2, 9.4, 9.9, 11.1	9.7
90	1.6, 1.8, 2.6, 2.7	2.2	2.0, 2.6, 2.7, 2.5	2.5	2.5, 4.0,4.3, 4.3	4.2

Table 2: Mass losses of each material as a function of angle of impingement

Angle of Impingement	Wear Scar Dimensions					
	Lost Wax Casting, Stellite 6		Sand Cast, Stellite 6		Stainless Steel 316	
	Depth/µm	Length/mm	Depth/µm	Length/mm	Depth/µm	Length/mm
20	26	12	24	12	72	14
45	71	6	76	5	194	9
60	95	5.5	94	5.8	115	7
90	20	6	24	6	40	7.8

Table 3: 2D surface profile scan dimensions

Highlights

1. Effect of impact angle on Stellite 6 and SS316 investigated at 20, 45, 60 and 90°.
2. Lost Wax and Sand Cast Stellite 6 presented similar erosion-corrosion resistance.
3. Stellite 6 had greater erosion-corrosion resistance over SS316.
4. SS316 had a more ductile response to angle of impact compared with Stellite 6.
5. Maximum mass loss SS316: 45°; Maximum mass loss both Stellite 6 casts: 60°.

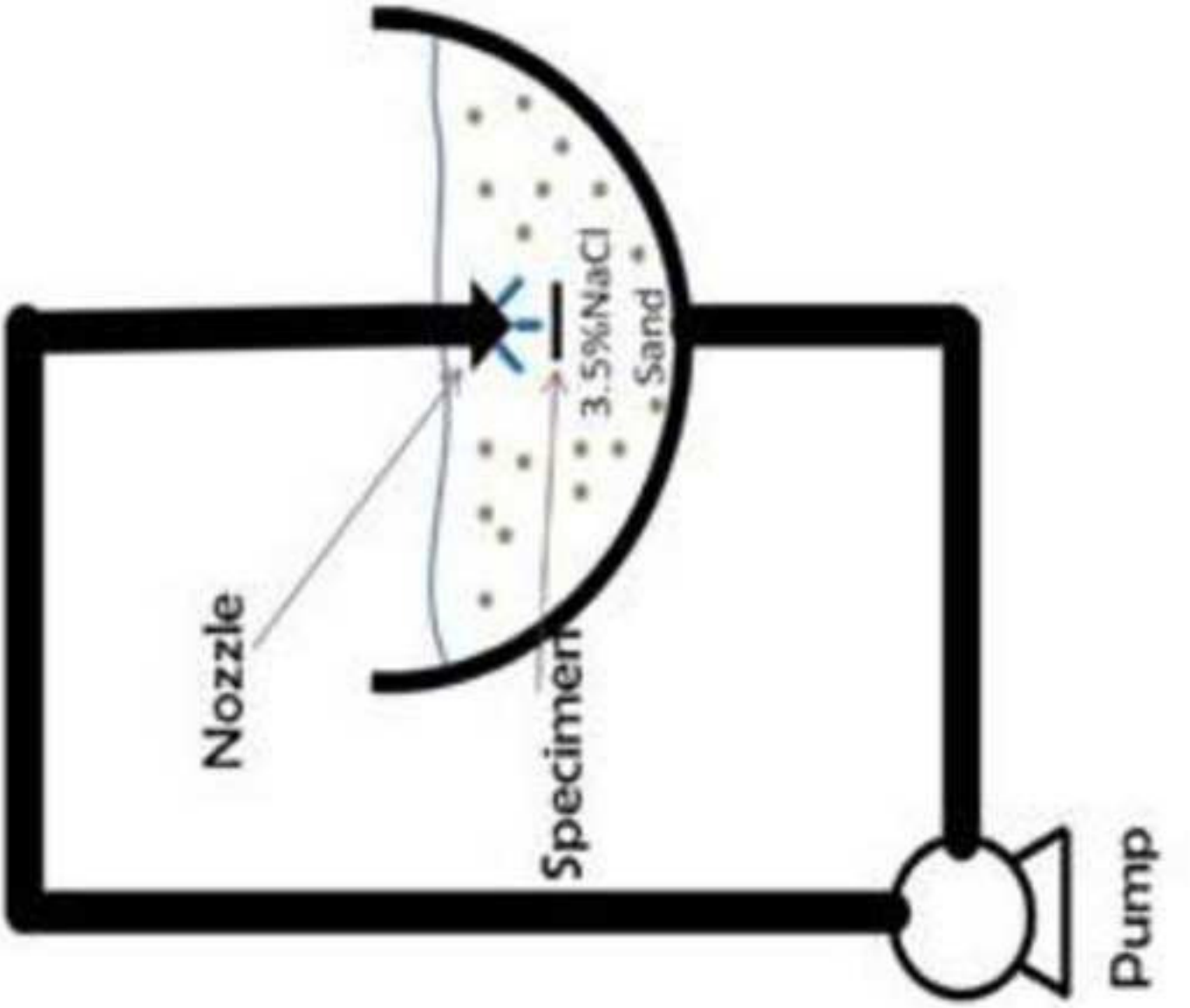

Figure 2

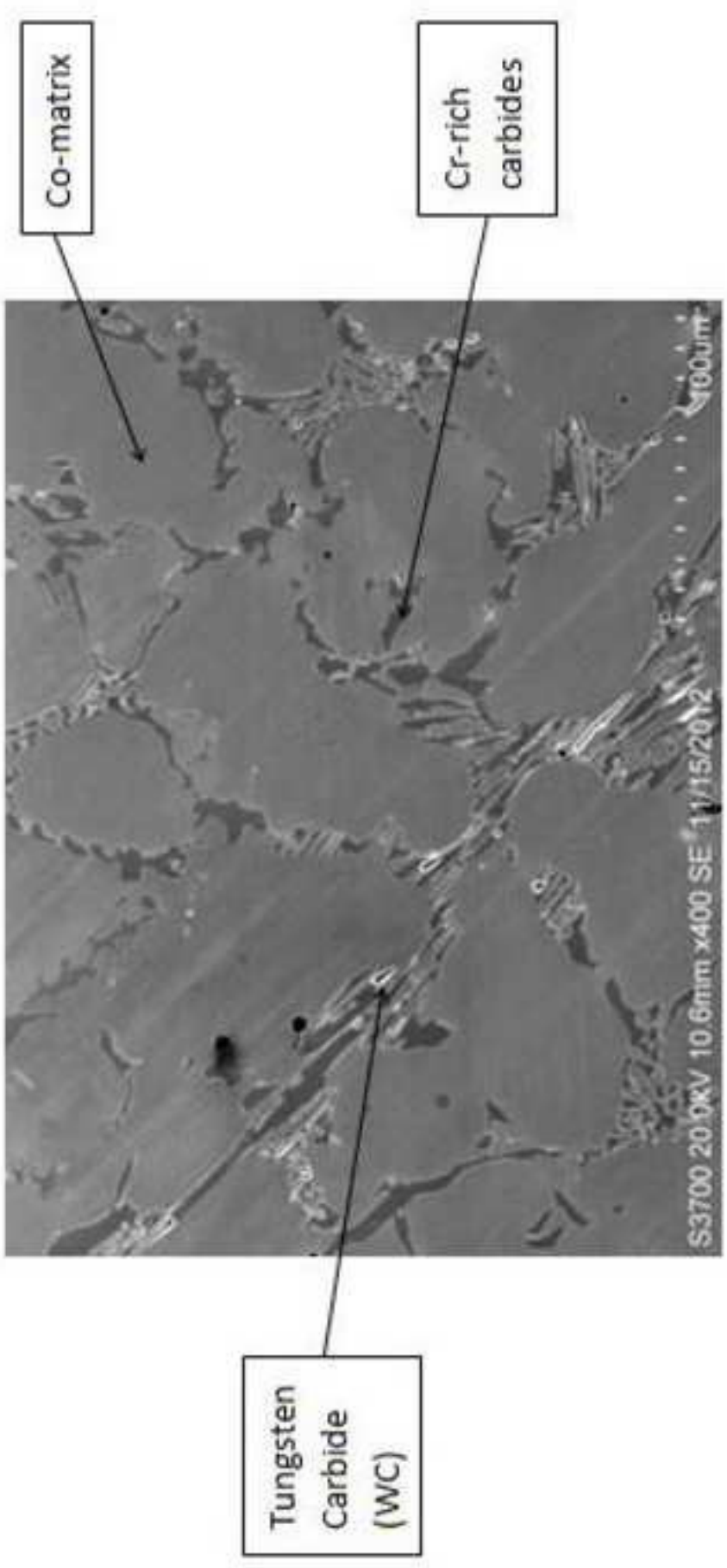
Co-matrix
Cr-rich carbides
Tungsten Carbide (WC)
S3700 20.0kV 10.6mm x400 SE 11/15/2012
100um

Figure 1

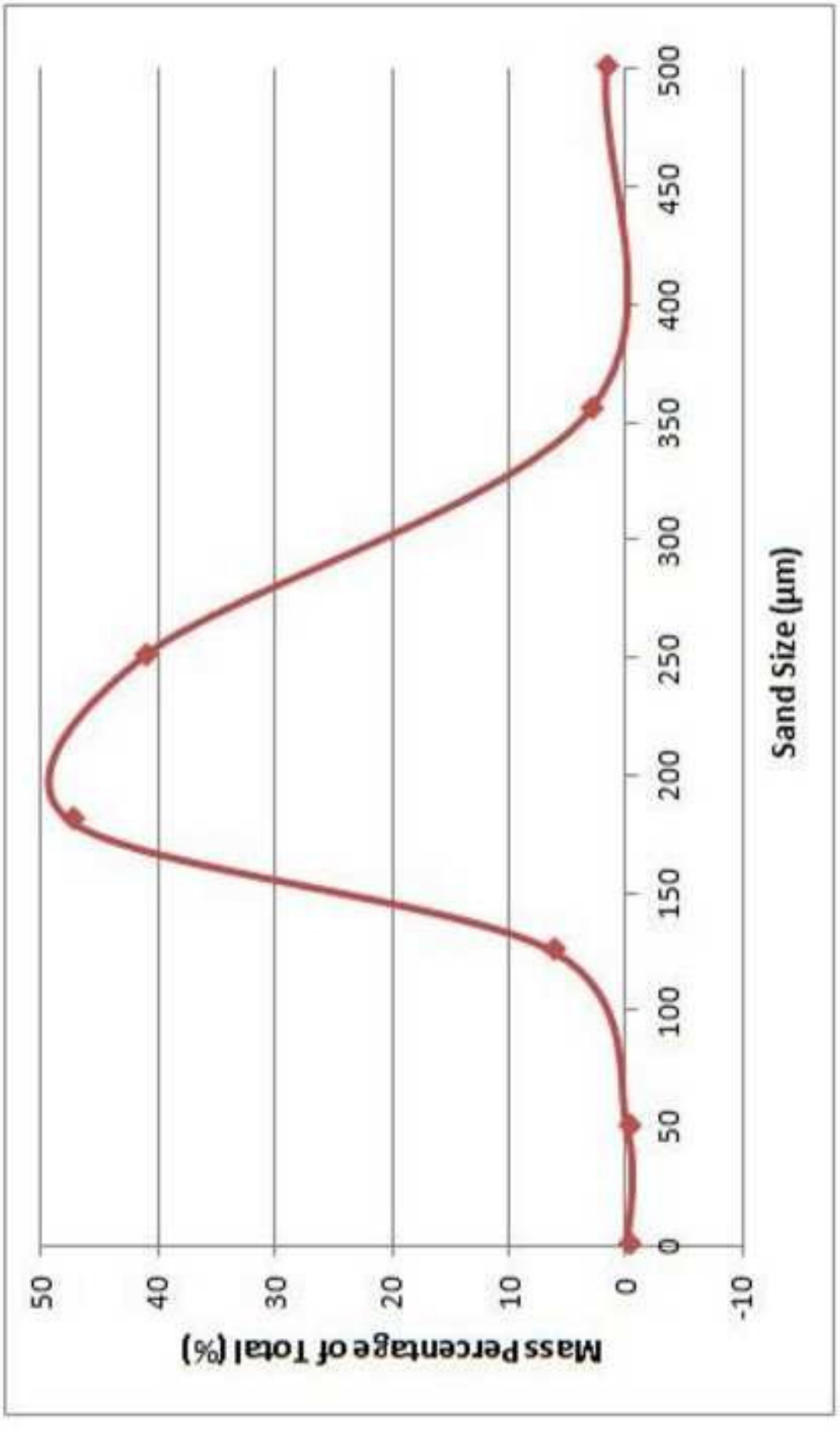
Mass Percentage of Total (%)
50
40
30
20
10
0
-10
0
50
100
150
200
250
300
350
400
450
500
Sand Size (µm)

Figure 3

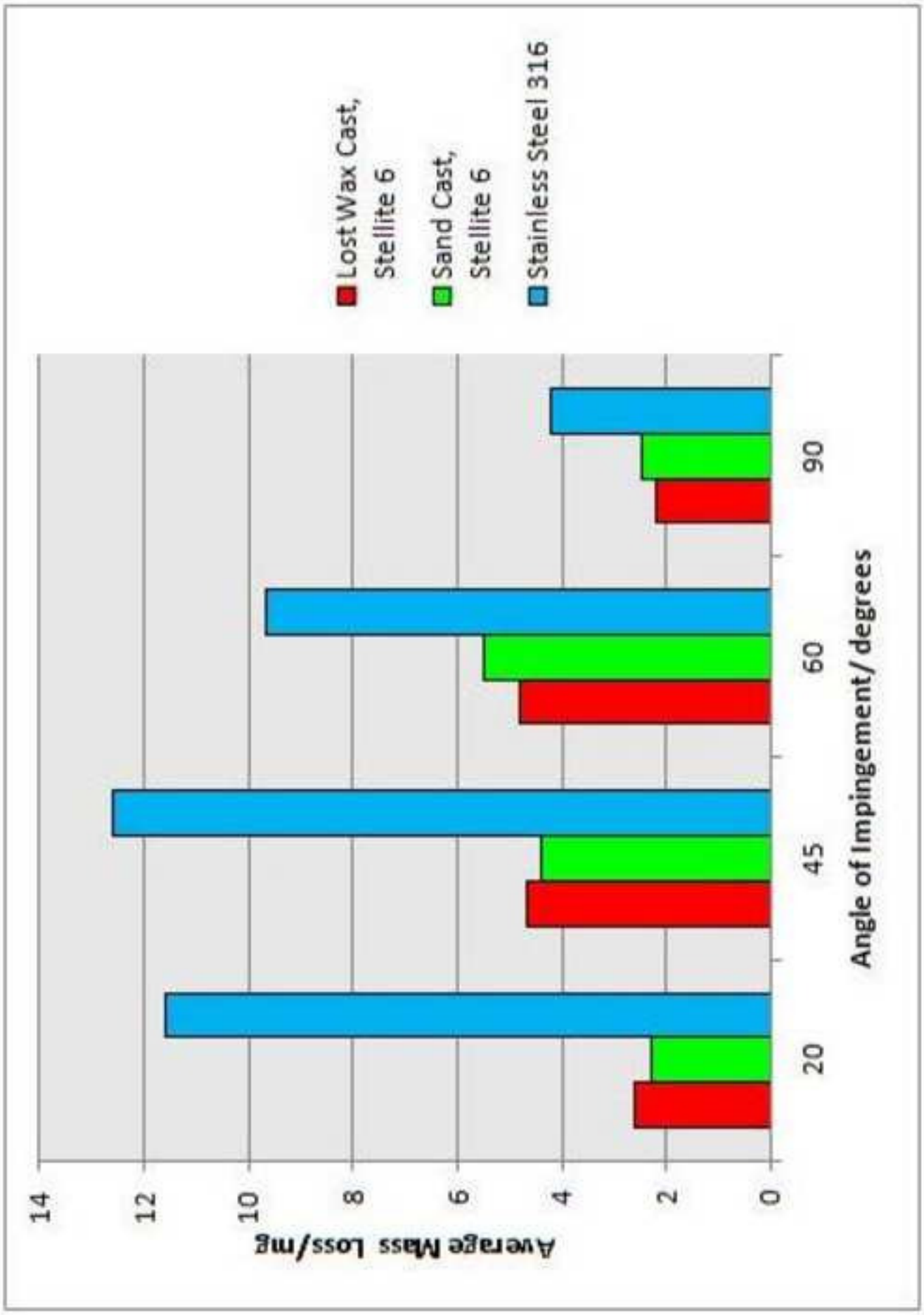
Lost Wax Cast, Stellite 6
Sand Cast, Stellite 6
Stainless Steel 316
Average Mass Loss/mg
0
2
4
6
8
10
12
14
20
45
60
90
Angle of Impingement/ degrees

Figure 4

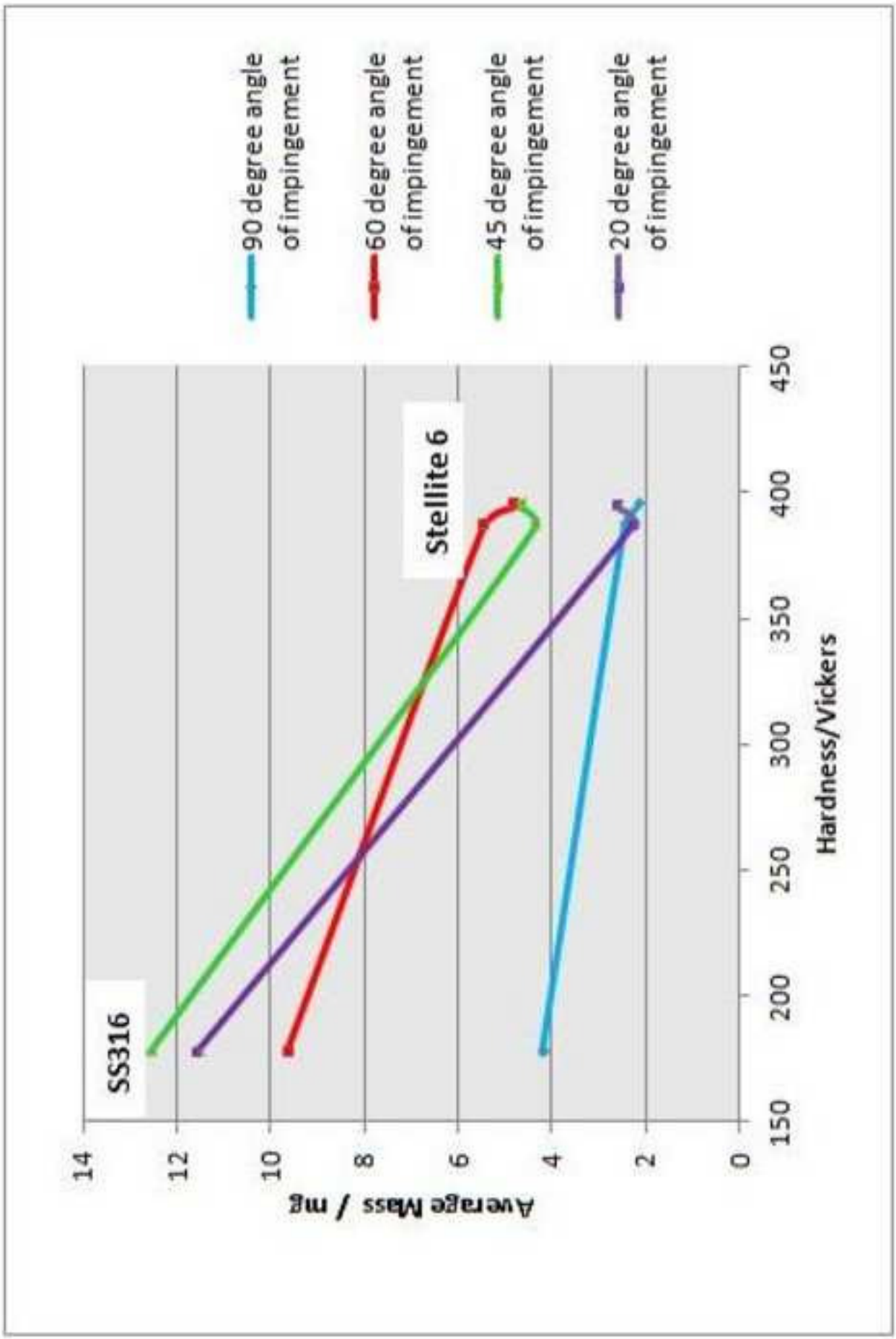
90 degree angle of impingement
60 degree angle of impingement
45 degree angle of impingement
20 degree angle of impingement
SS316
Stellite 6
Average Mass / mg
Hardness/Vickers
0
2
4
6
8
10
12
14
150
200
250
300
350
400
450

Figure 5

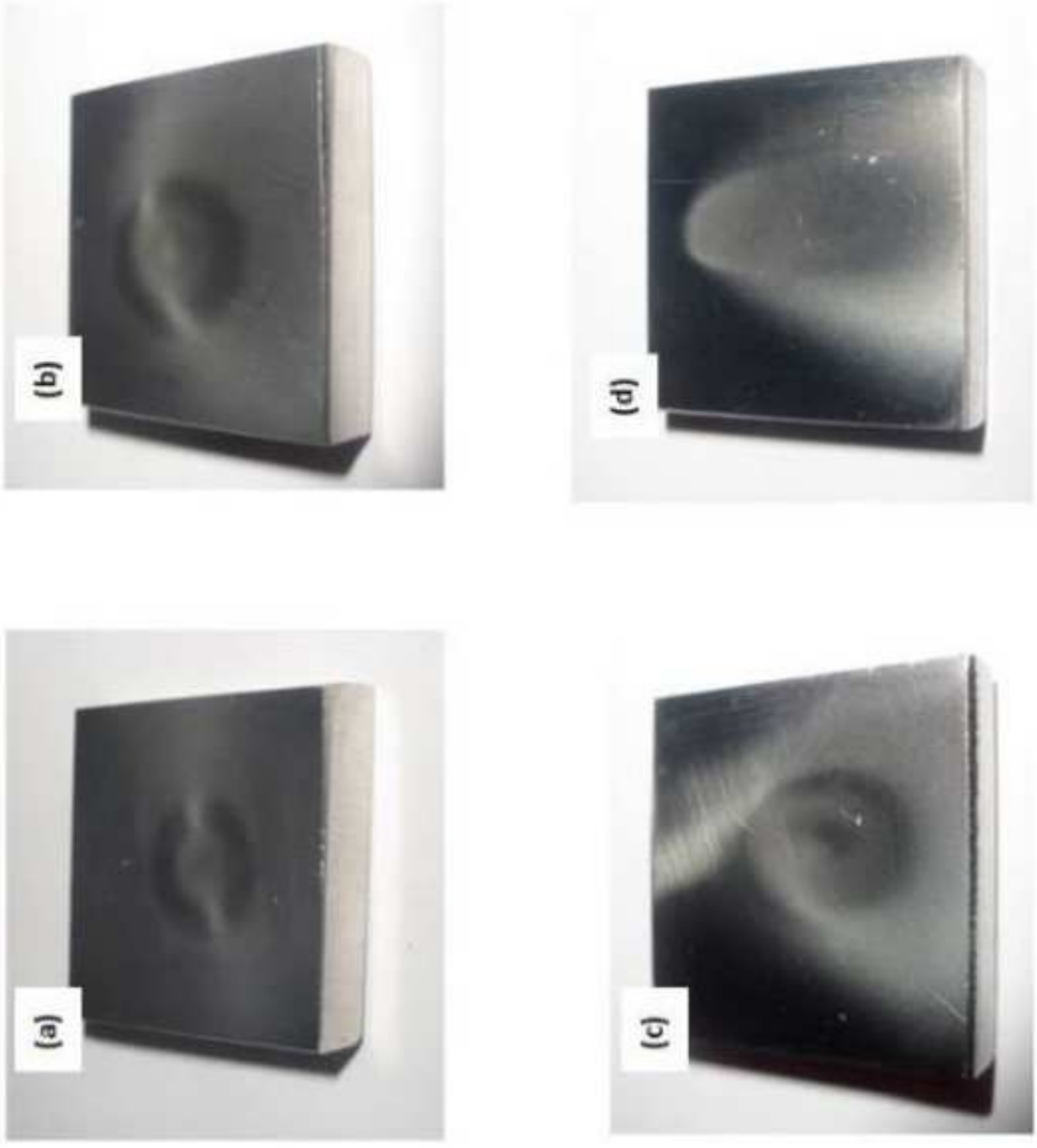

Figure 6

Figure 7

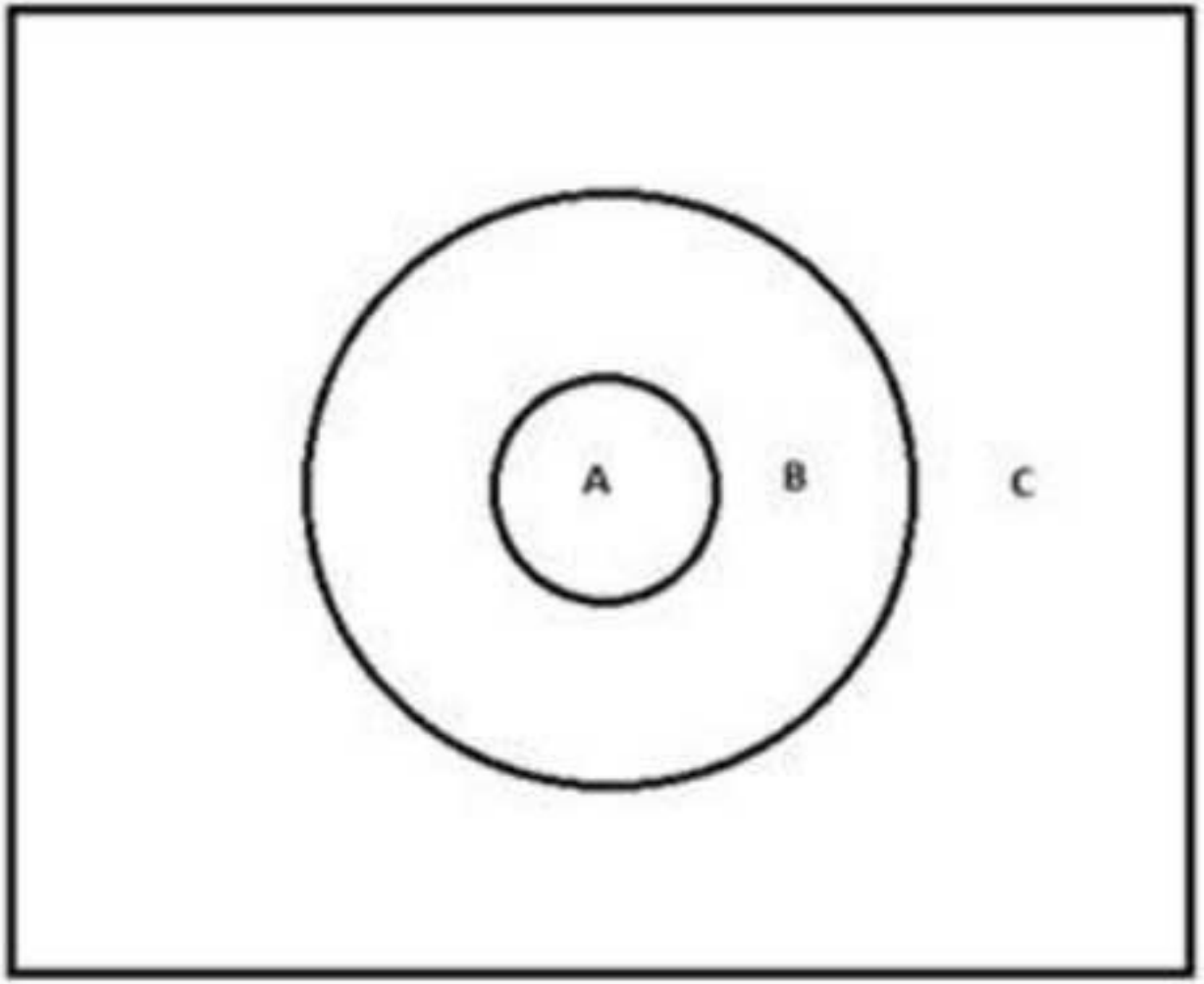

A - Direct Impingement Area

B - Tubulent Area

C - Outer Area

Figure 8

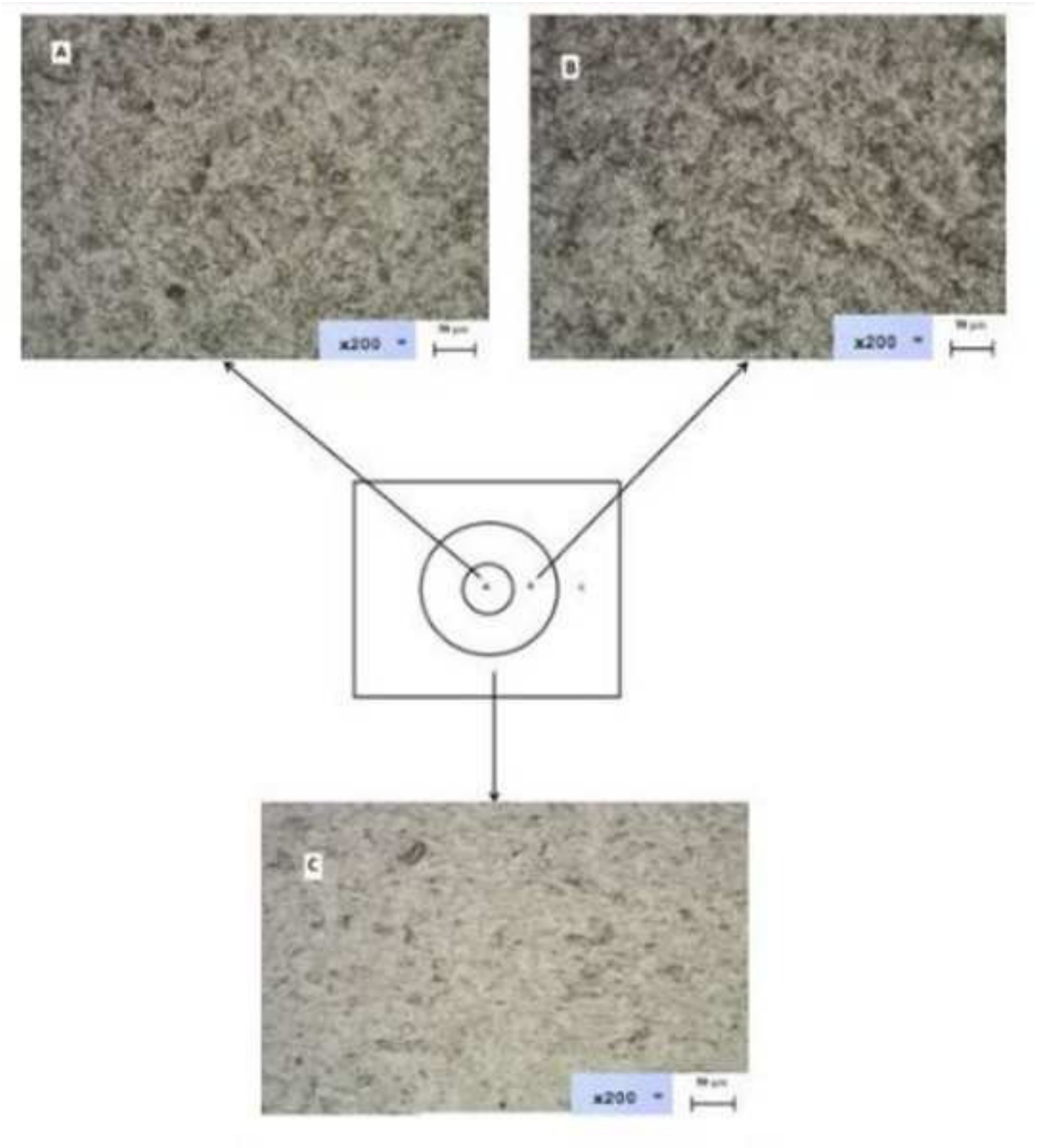

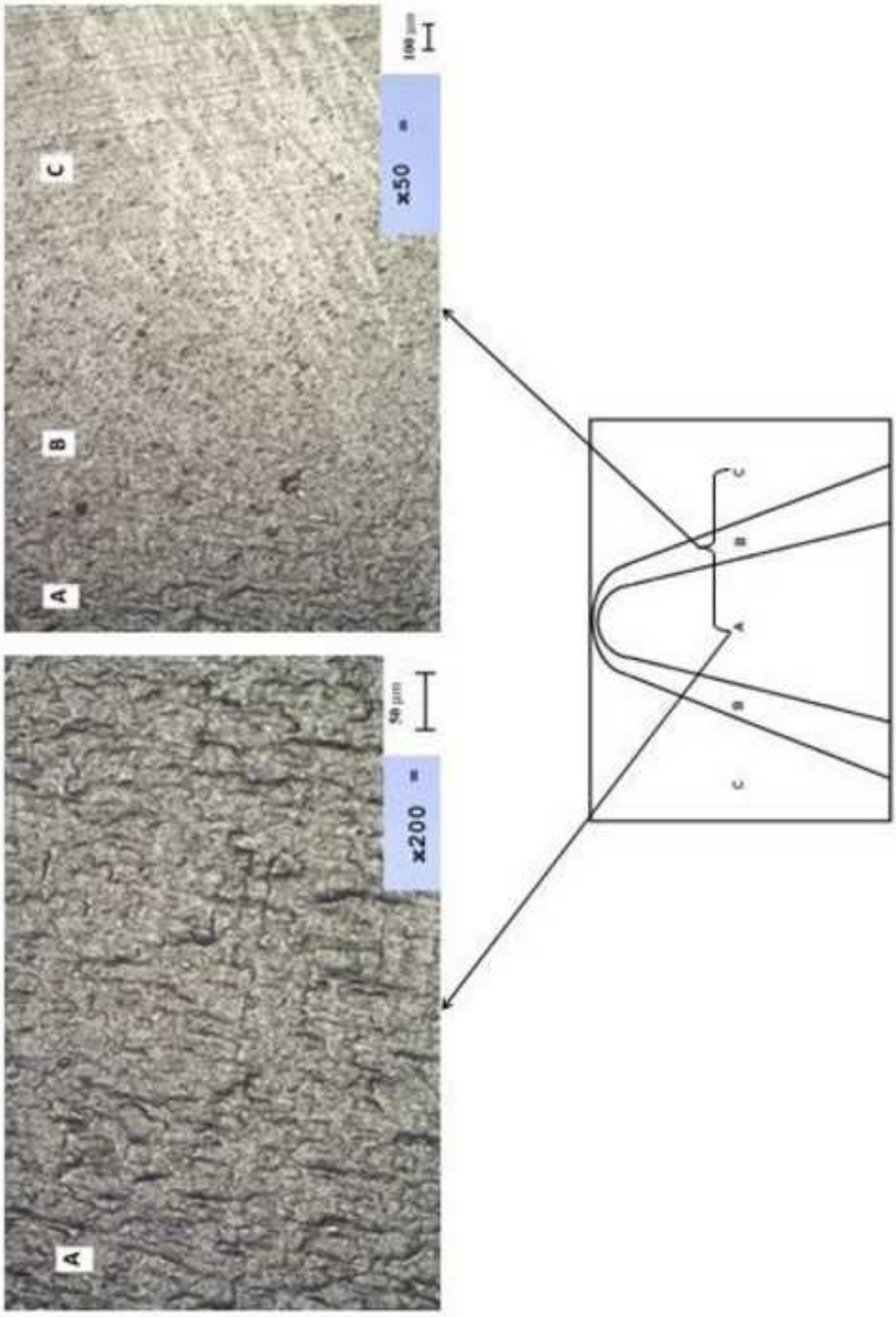

Figure 9

Figure 10

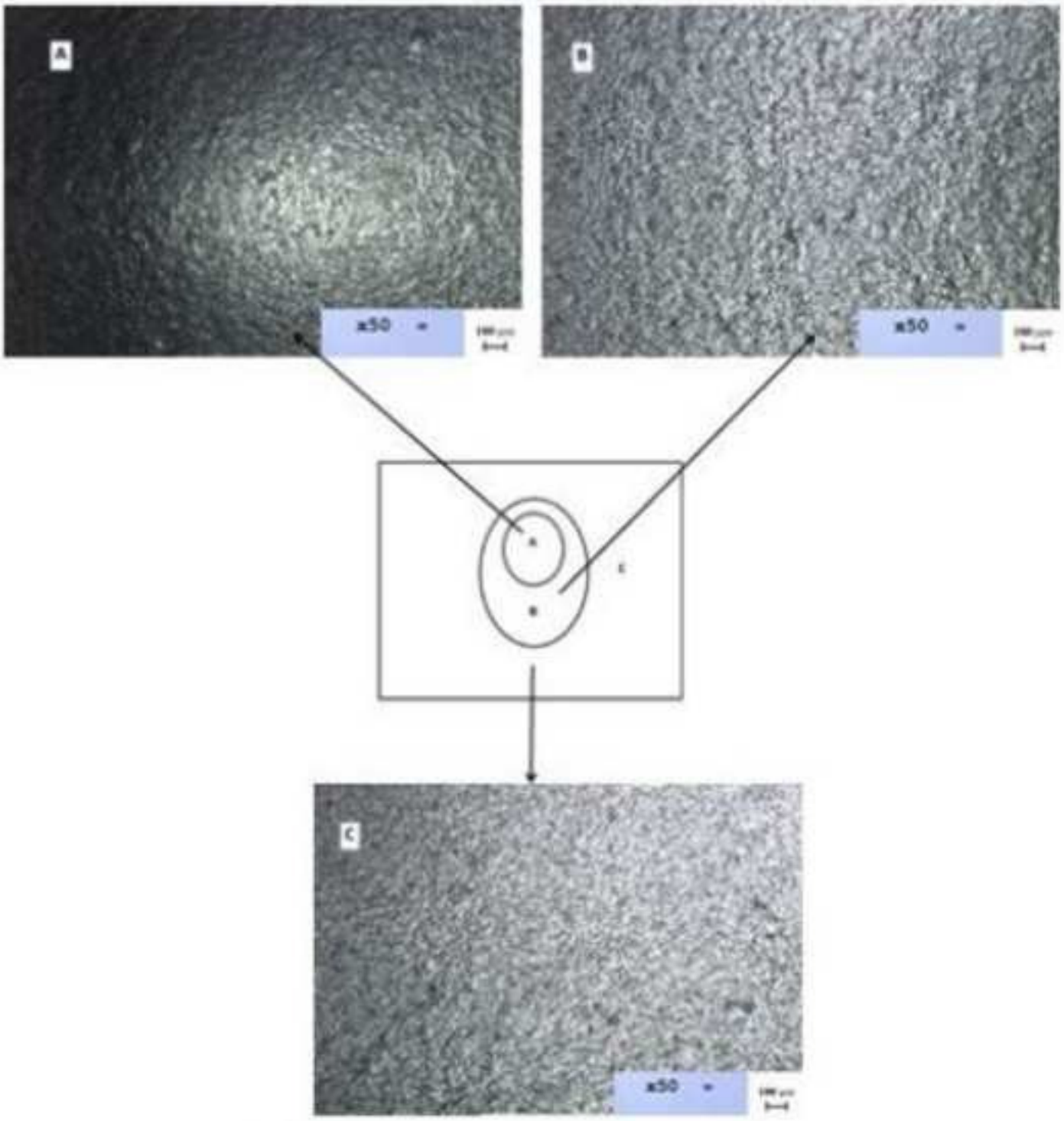

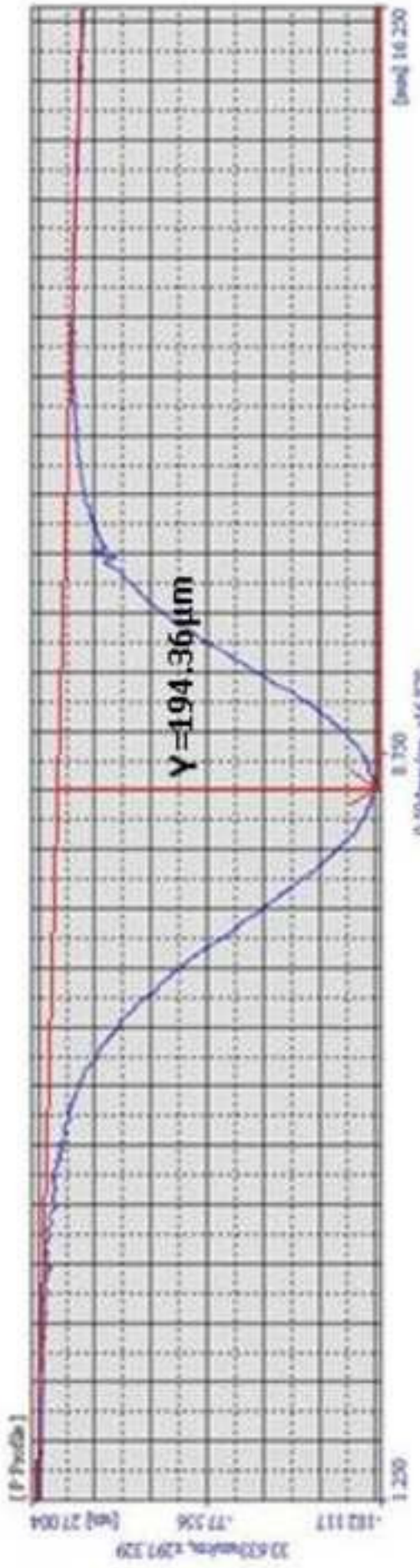

Figure 11

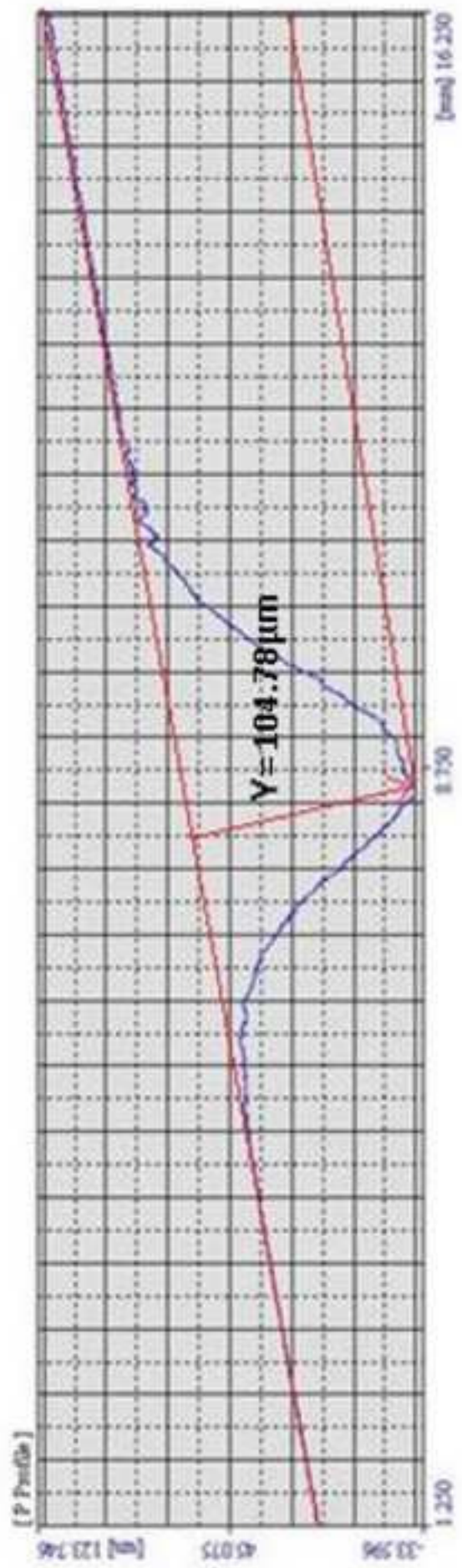

Figure 12

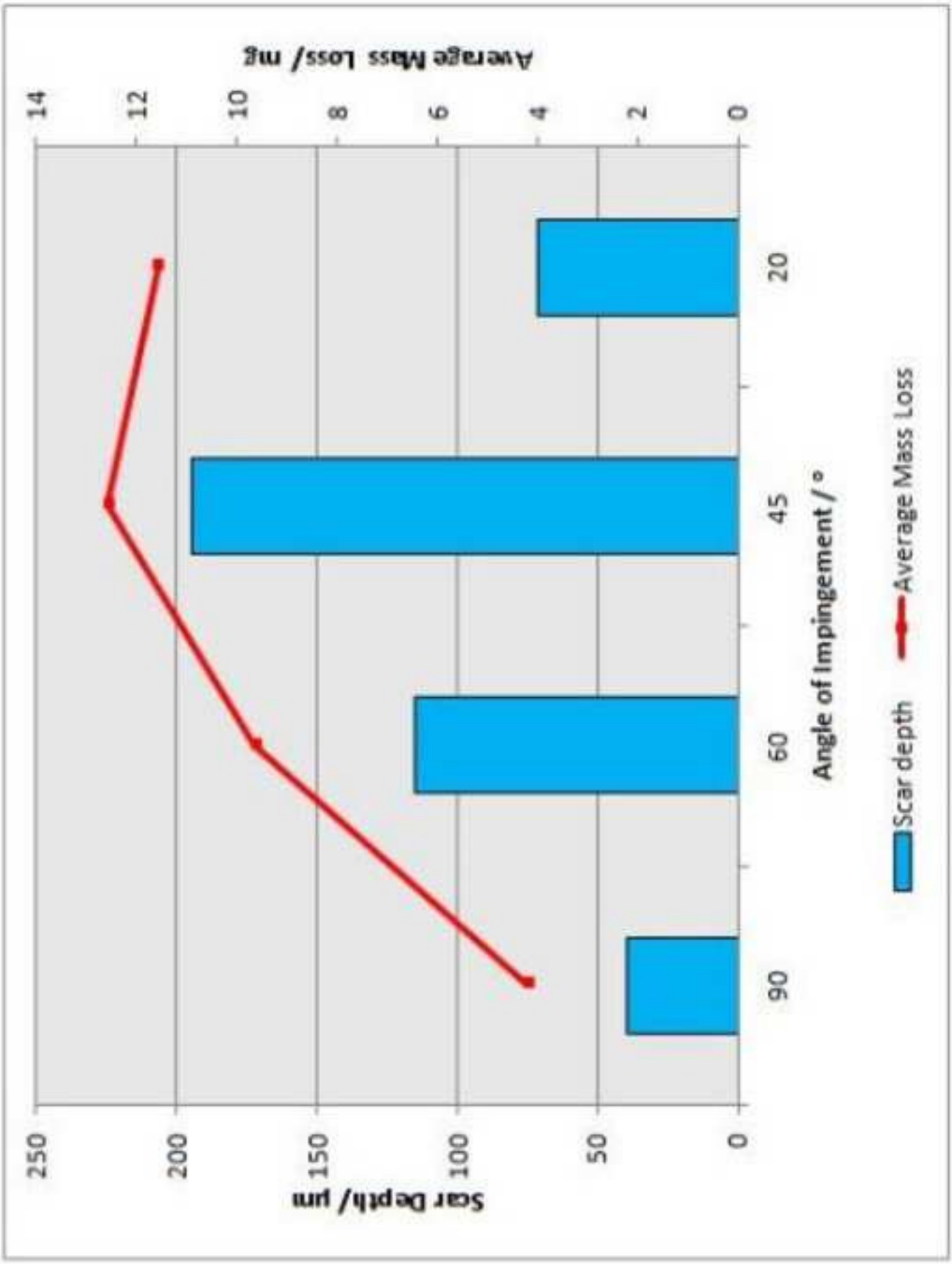
Average Mass Loss/ mg
14
12
10
8
6
4
2
0
Scar Depth/ μm
250
200
150
100
50
0
20
45
60
90
Angle of Impingement / °
Scar depth
Average Mass Loss

Figure 13

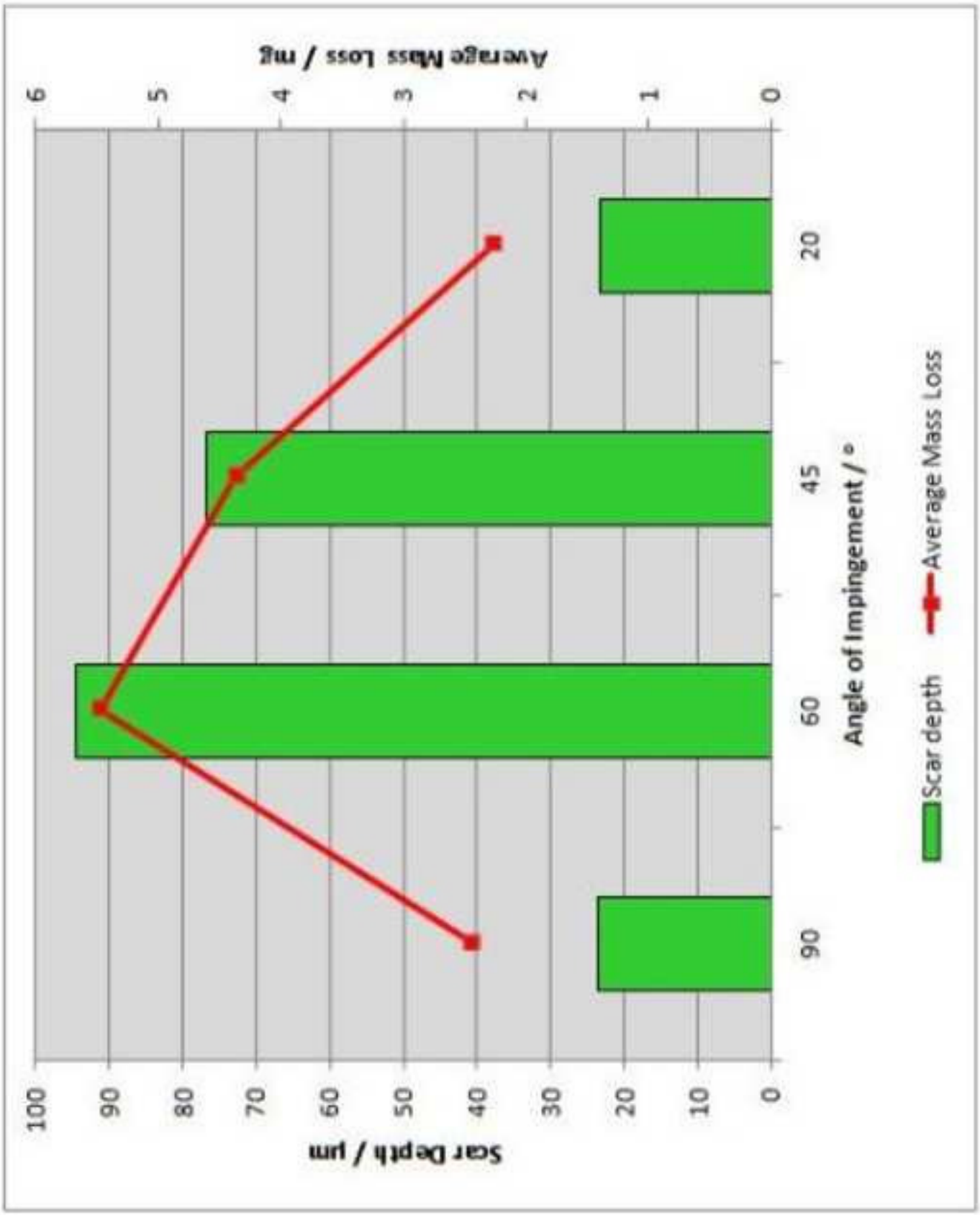
Scar Depth / μm
0
10
20
30
40
50
60
70
80
90
100
Average Mass Loss / mg
0
1
2
3
4
5
6
Angle of Impingement / °
20
45
60
90
Scar depth
Average Mass Loss

Figure 14

Figure 15

(a): Angular Sand before Experiment

(b): Angular Sand after Experiment